TELKOMNIKA Telecommunication, Computing, Electronics and Control
Vol. 18, No. 2, April 2020, pp. 631~639
ISSN: 1693-6930, accredited First Grade by Kemenristekdikti, Decree No: 21/E/KPT/2018
DOI: 10.12928/TELKOMNIKA.v18i2.14759

Development of triangular array eight patches antennas for circularly-polarized synthetic aperture radar sensor

Muhammad Fauzan Edy Purnomo[1], Vita Kusumasari[2], Edi Supriana[3], Rusmi Ambarwati[4], Akio Kitagawa[5]
[1,4]Department of Electrical Engineering, Brawijaya University, Indonesia
[2]Department of Mathematics, Universitas Negeri Malang, Indonesia
[3]Department of Physics, Universitas Negeri Malang, Indonesia
[5]Department of Electrical Engineering and Computer Science, Kanazawa University, Japan

Article Info

Article history:

Received Jul 29, 2019
Revised Jan 12, 2020
Accepted Feb 9, 2020

Keywords:

Corporate feeding-line
CP-SAR
LHCP and RHCP
MoM
UAV

ABSTRACT

In this paper, we obtain the left-handed circularly polarized (LHCP) and right-handed circularly polarized (RHCP) of triangular array eight patches antennas using corporate feeding-line for circularly polarized-synthetic aperture radar (CP-SAR) sensor embedded on unmanned aerial vehicle (UAV) with compact, simple, and efficient configuration. Although the corporate feeding-line design has already been developed, its design was for the side antenna view of 0° and only produced one of LHCP or RHCP instead of both. Here, the design for LHCP and RHCP eight patches array fed by corporate feeding-line having the side antenna view of 36° at *f*=1.25 GHz for CP-SAR are discussed. We use the 2016 version of computer simulation technology (CST) to realize the method of moments (MoM) for analyzing. The performance results, especially for gain and axial ratio (*Ar*) at resonant frequency are consecutively 13.46 dBic and 1.99 dB both of LHCP and RHCP. Moreover, the 12-dBic gain-bandwidth and the 3-dB *Ar*-bandwidth of them are consecutively around 38 MHz (3.04%) and 6 MHz (0.48%). Furthermore, the two-beams appeared at boresight in elevation plane for average beamwidth of 12 dBic-gain and the 3 dB-*Ar* LHCP and RHCP have similar values of around 12° and 46°, respectively.

Corresponding Author:

Muhammad Fauzan Edy Purnomo,
Department of Electrical Engineering,
Brawijaya University, 167 M. T. Haryono St., Malang 65145, Indonesia.
Email: mfauzanep@ub.ac.id

1. INTRODUCTION

There are two main types of radar images, which are the circularly scanning plan-position indicator (PPI) images and the side-looking images. The PPI applications are limited to monitor the air and naval traffic. Meanwhile, the side-looking images applied in remote sensing are divided into two types: (i) real aperture radar (RAR, usually called SLAR for side-looking airborne radar or SLR for side-looking radar), (ii) synthetic aperture radar (SAR). The radar captures a signal with a relatively low power level. In contrast to the other image techniques for instance RAR that uses the actual size of the antenna, SAR works with a comparatively small antenna which has a wide coverage area, high radiation efficiency, small conductive loss, and ease of excitation [1, 2]. The side antenna view is at the angle between 20° and 50°. This direction is called the range.

SAR is well-known as a multi-purpose sensor that can be operated in all weather and day-night time. Recently, many SAR sensors missions have been carried out in linear polarization (LP) such as horizontal-horizontal (HH), vertical-vertical (VV), and its combination with high power, sensitive to Faraday rotation effect, etc. [3, 4]. The interest in the SAR system is expected to increase research in the antenna that can be applied to the development of SAR system. The research aims to develop a technology that enables the transmission and reception of any information, such as images, imagery, topography, climate, etc. by using certain carrier media, i.e., unmanned aerial vehicle (UAV). There are many types of UAV based on the weight, size, and usage characteristics, such as heavy UAV, light UAV, medium UAV, small UAV, drone, microsatellite, etc. UAV is controlled directly by a device that have been programmed. It can transport SAR payloads such as flight control system, onboard computer, telemetry and command data handling, attitude controller, and sensor (including antenna both Transmitter, *Tx* and Receiver, *Rx*) [5]. Therefore, the platform of UAV is very perspective because it can be flown under the cloudy weather, unmanned, low cost, fast, and relatively low risk. Thus, UAV technology is a good alternative because the data obtained would be very detail and real-time, as well as could be acquired quickly with a lower price [6]. The SAR sensor employs the elliptical wave propagation and scatters the phenomenon by radiating and receiving the elliptically polarized wave, including different polarization as circular and linear polarization.

Moreover, the circularly polarized-synthetic aperture radar (CP-SAR) is as an active sensor that can transmit and receive the *C*, *S*, and *L*-band chirp pulses for remote sensing application. The sensor is designed as a low cost, light, low power, low profile configuration to transmit and receive left-handed circular polarization (LHCP) and right-handed circular polarization (RHCP), where the transmission and reception both work in LHCP and RHCP [4]. These circularly polarized waves are employed to generate the axial ratio image (ARI), ellipticity and tilted angle images, etc. Hence, any information can be obtained from the earth and be able to overcome some limitations of the SAR sensor, such as high power, sensitive to Faraday rotation effect, the unwanted backscatter modulation signal and redistribution random back signal-energy, blurring and defocusing spatial variants, ambiguous identification, and low different features of backscatter [7].

This paper presents the low power of triangular microstrip antenna for CP-SAR sensor application. This study involves developing array eight patches antennas that fundamentally construct the mold of substantial planar array using proximity coupled feed to yield the circular polarization (CP) rather than the other antennas operated in LP [8-10]. It is because the right pattern of basic construction determines the superiority of the designed array antenna using corporate feeding-line [11-14]. Although the corporate feeding-line design has already been developed [15, 16], its design was for the antenna view in the side of 0° angle and only produced one of LHCP or RHCP instead of both. Here, the design for LHCP and RHCP eight patches array fed by corporate feeding-line having low power and the antenna view in the side of 36° angle for CP-SAR application are discussed. Also, the study expresses that the modified lossless T-junction power divider 2×4 configurations both for LHCP and RHCP are capable of being reciprocal, matched, and lossless at all ports that become one of novelty in this paper. Hence, the contribution of this paper is to describe two models of CP i.e. LHCP and RHCP using corporate feeding-line with side antenna view of 36° that can work simultaneously as *Tx*/*Rx* for CP-SAR sensor application.

2. RESEARCH METHOD

The method of moments (MoM) is chosen in the numerical analysis for fast calculation. This method discretizes the integral into a matrix equation. This discretization can be considered as dividing the antenna surface into a small mesh [17]. To realize this method, we use computer simulation technology (CST) version 2016 from corporate company CST STUDIO SUITE [18]. The numerical simulation of the equilateral triangular array eight patches antennas with truncated-tip are shown in section 3, especially at the resonant frequency, f = 1.25 GHz as a simple configuration embedded on UAV for CP-SAR application both for *Tx* and *Rx*. Table 1 shows the specification and the desired target for the CP-SAR system [15], which influence the specification of the *L*-band CP-SAR UAV antenna. Each antenna can generate a wave that yields a CP. The technique to achieve CP can be easily obtained i.e. by adjusting the parameters properly (see Table 2), examining the size of perturbation segment, determining locus feed, and designing of corporate feeding [7, 11-12]. Therefore, the current distribution flow around patches that yield the significant variation performances of CP, especially *S*-parameter, frequency characteristic, input impedance, and radiation pattern.

This paper discusses and analyzes the design of LHCP and RHCP array eight patches antennas at *L*-band for CP-SAR sensor application embedded on the UAV. The characteristic performance of this antenna is CP, particularly a circular to the left that makes it easier to transmit and receive signals to/from the earth.

This antenna is made by using the type of microstrip antenna that uniquely structured, so that it complies with the technical specifications and the desired goal, especially as *Tx*/*Rx* of remote sensing application [13].

Table 1. Technical specification of CP-SAR on UAV

No	Antenna Parameters	Specification of CP-SAR on UAV
1	Resonant frequency (GHz)	1.25
2	Pulse band wide (MHz)	233.31
3	Axial ratio (dB)	≤ 3
4	Antenna efficiency (%)	> 80
5	Gain antenna (dBic)	12
6	Azimuth beamwidth (°)	≥ 6.77
7	Elevation beamwidth (°)	3.57 – 31.02
8	Antenna size (m)	0.7 × 0.4
9	Polarization (*Tx*/*Rx*)	LHCP + RHCP

Figure 1, Figure 2, and Table 2 show the configuration of an equilateral triangular array eight patches antennas with truncated-tip design including radiating patches and corporate feeding-line with their parameters [14]. Each of the radiating patches has the triangular shape of array antenna as the simple configuration of CP-SAR sensor. The parameter sizes of each patch (patch 1, patch 2, patch 3, patch 4, patch 5, patch 6, patch 7, and patch 8) are the same. Further, the corporate feeding-line has seven nodes of T-junction to distribute the current from the input port to radiating patches and reaches 2×4 patches which have the same length from the input port to radiating patches around 5.25λ or 854.7 mm. Then, the two orthogonal resonant modes of equal amplitudes and 90° phase difference with a compact TM_{21} CP operation on the resonant frequency at 1.25 GHz can be generated with a side-angle of 36° and create the stable radiation patterns which are slightly symmetric at the boresight beam. This case occurs because the location of corporate feeding-line is properly below the radiating patches which have the perturbation segment that make this construction different with other design [15, 16] and become a novelty for this research. Moreover, to examine the modified lossless T-junction power divider 2×4 configurations for both LHCP and RHCP as types of polarization approaching of reciprocal, matched, and lossless at all ports, it is given in the following explanation as proposed method for enhancing the performance of these antennas.

For nine ports power divider, isolation between output ports, for example, port 2 and port 3 (see Figure 1 and Figure 2), is essential for reducing cross-talk that can be caused by coupling between the ports [19-21]. By definition, a –9 dB power divider is an ideal passive lossless reciprocal nine ports device that divides power equally in magnitude and phase. The *S*-parameter matrix related to this device is (1).

$$S = [s_{ij}]_{9\times9} \tag{1}$$

According to the matrix in (1), the condition for a lossless network is given by (2).

$$S^T S^* = I \text{ or } (S^*)^T S = I \tag{2}$$

We define that S^T and S^* are a transpose and a conjugate matrix of *S*, respectively. The situation for a reciprocal network is described in (3).

$$S = S^T \text{ or } s_{ij} = s_{ji}\ ; \text{ for all } i \text{ and } j \tag{3}$$

Then, the condition for coefficient reflection load (Γ_L) is

$$\Gamma_L = 1 - |s_{ij}|^2 = \frac{reflection\ wave}{incident\ wave}; 0 \le \Gamma_L \le 1; i,j = 1,2,..,9 \tag{4}$$

If $\Gamma_L = 1\lfloor 0°$, then it occurs an open circuit condition. If $\Gamma_L = 1\lfloor 180°$, this is a short circuit condition. If $\Gamma_L = 0$, then this is a matched load circuit condition. Since all the nine ports of this power divider are matched, we have $s_{ii} = 0$ for matched load condition. In the *S*-matrix, the elements s_{23} and s_{32} are associated with the isolation between the output ports. These correspond to signals entering port 2 and exiting port 3, and vice versa. When the magnitudes of these elements are small, high isolation is achieved between the ports. For the lossless condition to be true, the *S*-matrix must be unitary and satisfy.

$$|s_{12}|^2 + |s_{13}|^2 + |s_{14}|^2 + |s_{15}|^2 + |s_{16}|^2 + |s_{17}|^2 + |s_{18}|^2 + |s_{19}|^2 = 1 \quad (5)$$

$$|s_{19}|^2 + |s_{29}|^2 + |s_{39}|^2 + |s_{49}|^2 + |s_{59}|^2 + |s_{69}|^2 + |s_{79}|^2 + |s_{89}|^2 = 1 \quad (6)$$

$$|s_{12}|^2 + |s_{23}|^2 + |s_{34}|^2 + |s_{45}|^2 + |s_{56}|^2 + |s_{67}|^2 + |s_{78}|^2 + |s_{89}|^2 = 1 \quad (7)$$

$$s_{19}{}^* s_{29} s_{39} s_{49} s_{59} s_{69} s_{79} s_{89} = 0 \quad (8)$$

$$s_{89}{}^* s_{78} s_{67} s_{56} s_{45} s_{34} s_{23} s_{12} = 0 \quad (9)$$

$$s_{12}{}^* s_{13} s_{14} s_{15} s_{16} s_{17} s_{18} s_{19} = 0 \quad (10)$$

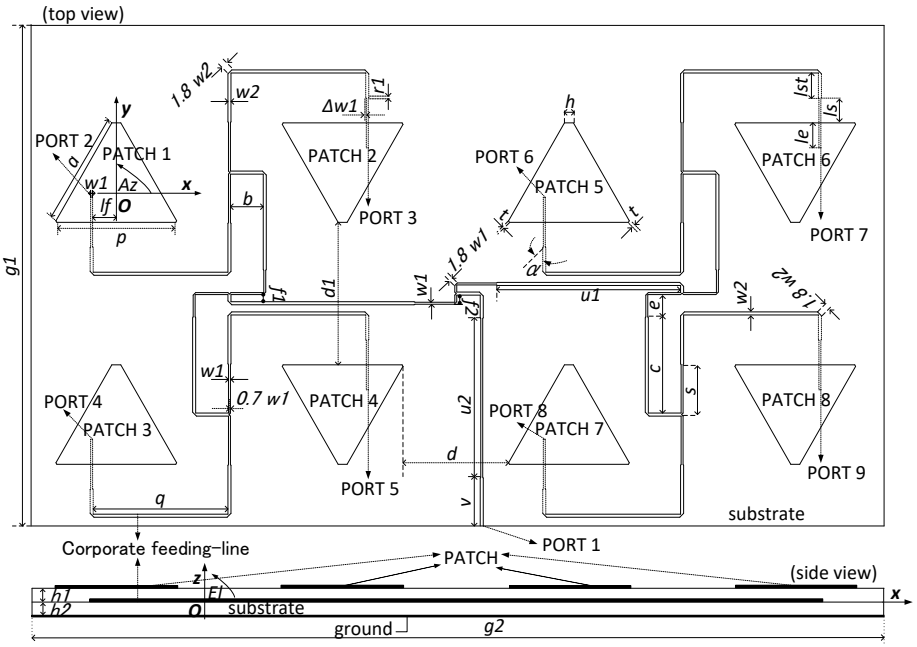

Figure 1. LHCP triangular array antenna 2×4

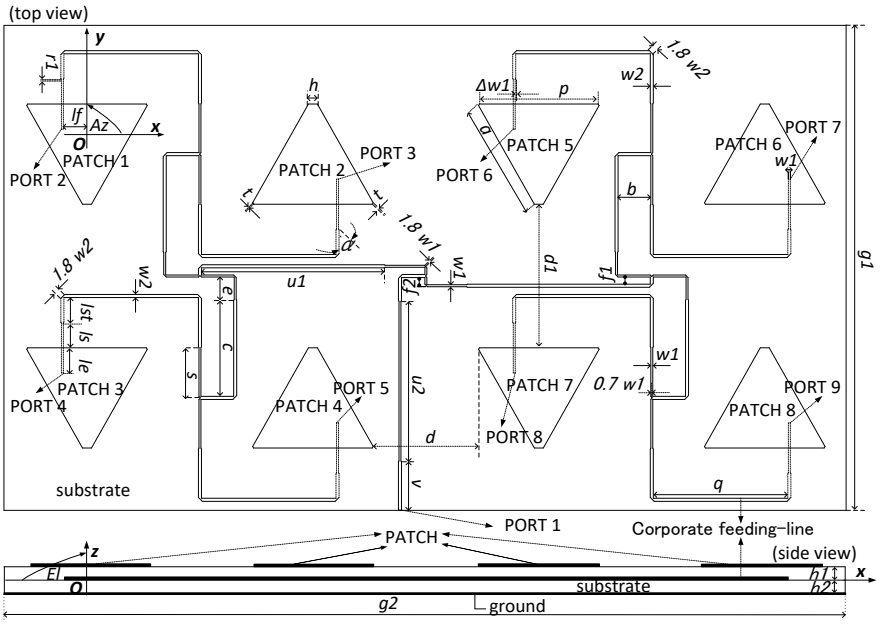

Figure 2. RHCP triangular array antenna 2×4

This case means that twenty of the elements s_{12}, s_{13}, s_{14}, s_{15}, s_{16}, s_{17}, s_{18}, s_{19}, s_{23}, s_{29}, s_{34}, s_{39}, s_{45}, s_{49}, s_{56}, s_{59}, s_{67}, s_{69}, s_{78}, s_{79}, and s_{89} must be equal to zero in order to satisfy (8)-(10). For more details of this analysis, s_{12}, s_{13}, s_{14}, s_{15}, s_{16}, s_{17}, s_{18}, and s_{19} set equal to zero. However, it is clear that by setting s_{12}, s_{13}, s_{14}, s_{15}, s_{16}, s_{17}, s_{18}, and s_{19}, equal to zero, (6) is not satisfied. Consequently, when twenty of the elements s_{12}, s_{13}, s_{14}, s_{15}, s_{16}, s_{17}, s_{18}, s_{19}, s_{23}, s_{29}, s_{34}, s_{39}, s_{45}, s_{49}, s_{56}, s_{59}, s_{67}, s_{69}, s_{78}, s_{79}, and s_{89} are equal to zero, one of the (5)-(7) will not be satisfied. Thus a matched, reciprocal, lossless of nine ports network becomes impossible to realize [22-25].

Table 2. The parameters of triangular array antenna 2×4

No.	Parameters	Values	No.	Parameters	Values
1	*a*	95.2311 mm	17	*q*	114.855 mm
2	*p*	101.38 mm	18	*b*	27.96 mm
3	*h*	7.64 mm	19	*c*	80.2 mm
4	*t*	1.5008 mm	20	*d*	90 mm
5	*s*	40.7 mm	21	*d1*	120 mm
6	*w1*	1.67 mm	22	*e*	18.755 mm
7	*w2*	2.59 mm	23	*f1*	6 mm
8	*⊿w1*	0.46 mm	24	*f2*	5.545 mm
9	α	30°	25	*u1*	150.5 mm
10	*le*	21 mm	26	*u2*	133.5 mm
11	*ls*	21 mm	27	*v*	40.3 mm
12	*r1*	0.4 mm	28	*g1*	400 mm
13	*lst*	20.6 mm	29	*g2*	700 mm
14	*lf*	20.17 mm	30	ε_r	2.17
15	*h1*	1.6 mm	31	δ	0.0005
16	*h2*	1.6 mm			

3. RESULTS AND ANALYSIS

3.1. The results of LHCP and RHCP modified lossless T-junction power divider 2×4

The real and imaginary parts of *S*-matrix based on (3) and (4), when the radiating patches are excluded and only the modified lossless T-junction power divider 2×4 networks both of LHCP (Figure 1) and RHCP (Figure 2) are operated in CST software at f = 1.25 GHz, are shown in (11) and (12) [26].

$$S_{LHCP} = \begin{bmatrix} 0.21+j\,0.02 & -0.12+j0.28 & -0.11+j\,0.28 & -0.15+j\,0.33 & -0.07+j\,0.34 & -0.09+j\,0.34 & -0.16+j0.32 & -0.13+j\,0.28 & -0.13+j\,0.28 \\ -0.12+j\,0.28 & -0.3-j\,0.2 & 0.65+j0.07 & -0.25+j0.19 & -0.26+j\,0.25 & 0.11-j\,0.06 & 0.12-j\,0.04 & 0.1-j0.04 & 0.1-j\,0.04 \\ -0.11+j\,0.28 & 0.65+j0.07 & -0.27-j\,0.2 & -0.26+j\,0.2 & -0.26+j\,0.25 & 0.11-j\,0.06 & 0.12-j\,0.04 & 0.1-j\,0.04 & 0.1-j\,0.04 \\ -0.15+j\,0.33 & -0.25+j\,0.19 & -0.26+j0.2 & -0.36-j\,0.22 & 0.57+j\,0.12 & 0.12-j0.07 & 0.14-j0.04 & 0.12-j\,0.04 & 0.12-j\,0.04 \\ -0.07+j\,0.34 & -0.26+j0.25 & -0.26+j0.25 & 0.57+j\,0.12 & -0.36-j0.09 & 0.11-j\,0.09 & 0.12-j\,0.07 & 0.11-j\,0.06 & 0.11-j\,0.06 \\ -0.09+j\,0.34 & 0.11-j\,0.06 & 0.11-j\,0.06 & 0.12-j0.07 & 0.11-j\,0.09 & -0.37-j0.1 & 0.56+j\,0.1 & -0.27+j0.25 & -0.26+j\,0.24 \\ -0.16+j\,0.32 & 0.12-j\,0.04 & 0.12-j\,0.04 & 0.14-j\,0.04 & 0.12-j\,0.07 & 0.56+j\,0.1 & -0.36-j\,0.23 & -0.26+j\,0.19 & -0.26+j\,0.19 \\ -0.13+j\,0.28 & 0.1-j\,0.04 & 0.1-j\,0.04 & 0.12-j\,0.04 & 0.11-j\,0.06 & -0.27+j\,0.25 & -0.26+j\,0.19 & -0.28-j\,0.21 & 0.65+j\,0.06 \\ -0.13+j\,0.28 & 0.1-j\,0.04 & 0.1-j\,0.04 & 0.12-j\,0.04 & 0.11-j\,0.06 & -0.26+j\,0.24 & -0.26+j\,0.19 & 0.65+j\,0.06 & -0.3-j\,0.21 \end{bmatrix} \quad (11)$$

We define that $S^T{}_{LHCP}$ and $S^*{}_{LHCP}$ are a transpose and a conjugate matrix of (11), respectively.

$$S_{RHCP} = \begin{bmatrix} 0.21+j\,0.02 & -0.16+j0.32 & -0.09+j\,0.34 & -0.13+j\,0.28 & -0.13+j\,0.28 & -0.11+j\,0.28 & -0.12+j0.28 & -0.07+j\,0.34 & -0.15+j\,0.33 \\ -0.16+j\,0.32 & -0.37-j\,0.23 & 0.56+j0.1 & -0.26+j0.19 & -0.27+j\,0.19 & 0.12-j\,0.04 & 0.12-j\,0.04 & 0.13-j0.07 & 0.14-j\,0.04 \\ -0.09+j\,0.34 & 0.56+j0.1 & -0.37-j\,0.1 & -0.26+j\,0.24 & -0.27+j\,0.24 & 0.11-j\,0.06 & 0.11-j\,0.06 & 0.12-j\,0.09 & 0.13-j\,0.07 \\ -0.13+j\,0.28 & -0.26+j\,0.19 & -0.26+j0.24 & -0.3-j\,0.21 & 0.64+j\,0.06 & 0.1-j0.04 & 0.1-j0.03 & 0.12-j\,0.06 & 0.12-j\,0.04 \\ -0.13+j\,0.28 & -0.27+j0.19 & -0.27+j0.24 & 0.64+j\,0.06 & -0.28-j0.21 & 0.1-j\,0.04 & 0.1-j\,0.03 & 0.11-j\,0.06 & 0.12-j\,0.04 \\ -0.11+j\,0.28 & 0.12-j\,0.04 & 0.11-j\,0.06 & 0.1-j0.04 & 0.1-j\,0.04 & -0.28-j0.2 & 0.65+j\,0.06 & -0.26+j0.25 & -0.26+j\,0.19 \\ -0.12+j\,0.28 & 0.12-j\,0.04 & 0.11-j\,0.06 & 0.1-j\,0.03 & 0.1-j\,0.03 & 0.65+j\,0.06 & -0.3-j\,0.2 & -0.26+j\,0.25 & -0.26+j\,0.19 \\ -0.07+j\,0.34 & 0.13-j\,0.07 & 0.12-j\,0.09 & 0.12-j\,0.06 & 0.11-j\,0.06 & -0.26+j\,0.25 & -0.26+j\,0.25 & -0.36-j\,0.09 & 0.57+j\,0.11 \\ -0.15+j\,0.33 & 0.14-j\,0.04 & 0.13-j\,0.07 & 0.12-j\,0.04 & 0.12-j\,0.04 & -0.26+j\,0.19 & -0.26+j\,0.19 & 0.57+j\,0.11 & -0.36-j\,0.22 \end{bmatrix} \quad (12)$$

Also, we notice that $S^T{}_{RHCP}$ and $S^*{}_{RHCP}$ are consecutively a transpose and a conjugate matrix of (12). For reciprocity, they are clear for both LHCP and RHCP, i.e., $S_{LHCP} = S^T{}_{LHCP}$ and $S_{RHCP} = S^T{}_{RHCP}$.

The matched ports of the divider set for LHCP s_{11} = 0.21 + j0.02, s_{22} = –0.3 – j0.2, s_{33} = –0.27 – j0.2, s_{44} = –0.36 – j0.22, s_{55} = –0.36 – j0.09, s_{66} = –0.37 – j0.1, s_{77} = –0.36 – j0.23, s_{88} = –0.28 – j0.21, and s_{99} = –0.3 – j0.21 and for RHCP s_{11} = 0.21 + j0.02, s_{22} = –0.37 – j0.23, s_{33} = –0.37 – j0.1, s_{44} = –0.3 – j0.21, s_{55} = –0.28 – j0.21, s_{66} = –0.28 – j0.2, s_{77} = –0.3 – j0.2, s_{88} = –0.36 – j0.09, and s_{99} = –0.36 – j0.22 are relatively close to zero. It means that only a little of the incident waves on the matched port will be reflected or not exit the ports. Thus, the reflected waves at the ports will close to zero. We get that both LHCP and RHCP are almost the lossless of the power divider in (2) and fulfill (5)-(10) as seen in (13) and (14).

$$S^T S^*_{LHCP} = \begin{bmatrix} 0.922 & 0.0012+j\,0.0052 & -0.0047+j\,0.0147 & 0.0018+j\,0.0098 & -0.0037+j\,0.019 & -0.0026+j\,0.0105 & -0.002+j\,0.0149 & -0.0048+j\,0.0142 & -0.0065+j\,0.0111 \\ 0.0012-j\,0.0052 & 0.9338 & -0.0189+j\,0.0055 & -0.0146+j\,0.0048 & -0.007+j\,0.0025 & 0.0138+j\,0.0027 & 0.0191+j\,0.0006 & 0.0125-j\,0.0006 & 0.0122+j\,0.0007 \\ -0.0047-j\,0.0147 & -0.0189-j\,0.0055 & 0.9234 & -0.0157+j\,0.0019 & -0.02-j\,0.0015 & 0.0143+j\,0.0016 & 0.0193-j\,0.0004 & 0.0126-j\,0.0014 & 0.0123-j\,0.0001 \\ 0.0018-j\,0.0098 & -0.0146-j\,0.0048 & -0.0157-j\,0.0019 & 0.9274 & -0.0245-j\,0.0064 & 0.0241+j\,0.0104 & 0.0126+j0.0013 & 0.0229+j\,0.0002 & 0.0224+j\,0.0015 \\ -0.0037-j\,0.019 & -0.007-j\,0.0025 & -0.02+j\,0.0015 & -0.0245+j\,0.0064 & 0.9286 & 0.0040-j\,0.0000 & 0.0212-j\,0.0084 & 0.0147-j\,0.0032 & 0.0145-j\,0.0018 \\ -0.0026-j\,0.0105 & 0.0138-j\,0.0027 & 0.0143-j\,0.0016 & 0.0241-j\,0.0104 & 0.004-j\,0.0000 & 0.9257 & -0.0174+j\,0.0078 & -0.0148+j\,0.0029 & -0.0189+j\,0.0054 \\ -0.002-j\,0.0149 & 0.0191-j\,0.0006 & 0.0193+j\,0.0004 & 0.0126-j\,0.0013 & 0.0212+j\,0.0084 & -0.0174-j\,0.0078 & 0.914 & -0.0276-j\,0.0024 & -0.0178+j0.0004 \\ -0.0048-j\,0.0142 & 0.0125+j\,0.0006 & 0.0126+j\,0.0014 & 0.0229-j\,0.0002 & 0.0147+j\,0.0032 & -0.0148-j\,0.0029 & -0.0276+j\,0.0024 & 0.9379 & -0.0181-j\,0.0014 \\ -0.0065-j\,0.0111 & 0.0122-j\,0.0007 & 0.0123+j\,0.0001 & 0.0224-j\,0.0015 & 0.0145+j\,0.0018 & -0.0189-j\,0.0054 & -0.0178-j\,0.0004 & -0.0181+j\,0.0014 & 0.9393 \end{bmatrix} \approx \begin{bmatrix} 1&0&0&0&0&0&0&0&0 \\ 0&1&0&0&0&0&0&0&0 \\ 0&0&1&0&0&0&0&0&0 \\ 0&0&0&1&0&0&0&0&0 \\ 0&0&0&0&1&0&0&0&0 \\ 0&0&0&0&0&1&0&0&0 \\ 0&0&0&0&0&0&1&0&0 \\ 0&0&0&0&0&0&0&1&0 \\ 0&0&0&0&0&0&0&0&1 \end{bmatrix} \quad (13)$$

$$S^T S^*_{RHCP} = \begin{bmatrix} 0.922 & 0.0002+j\,0.0123 & -0.0076+j\,0.0159 & -0.0031+j\,0.0129 & -0.0025+j\,0.0085 & -0.0097+j\,0.0092 & 0.0055+j0.0034 & -0.0108+j\,0.0269 & -0.0041+j\,0.0086 \\ 0.0002-j\,0.0123 & 0.9291 & -0.0184-j\,0.0072 & -0.017-j\,0.0003 & -0.0162+j\,0.0028 & 0.0141+j\,0.0001 & 0.0171+j\,0.003 & 0.015+j\,0.01 & 0.0212+j\,0.0006 \\ -0.0076-j\,0.0159 & -0.0184+j\,0.0072 & 0.9256 & -0.0139-j\,0.0045 & -0.013-j\,0.0015 & 0.0097-j\,0.0041 & 0.0132-j\,0.001 & 0.0067+j\,0.0023 & 0.0233-j\,0.0087 \\ -0.0031-j\,0.0129 & -0.017+j\,0.0003 & -0.0139+j\,0.0045 & 0.928 & -0.0117-j\,0.0025 & 0.0091+j\,0.0063 & 0.0043-j0.0086 & 0.0045+j\,0.0029 & 0.0262-j\,0.0007 \\ -0.0025-j\,0.0085 & -0.0162-j\,0.0028 & -0.013+j\,0.0015 & -0.0117+j\,0.0025 & 0.9247 & 0.0114+j\,0.0086 & 0.0066-j\,0.0065 & 0.0172+j\,0.0043 & 0.0202+j\,0.0001 \\ -0.0097-j\,0.0092 & 0.0141-j\,0.0001 & 0.0097+j\,0.0041 & 0.0091-j\,0.0063 & 0.0114-j\,0.0086 & 0.9237 & -0.0215-j\,0.006 & -0.0197-j\,0.0061 & -0.0187+j\,0.0034 \\ 0.0055-j\,0.0034 & 0.0171-j\,0.0030 & 0.0132+j\,0.001 & 0.0043+j\,0.0086 & 0.0066+j\,0.0065 & -0.0215+j\,0.006 & 0.9362 & -0.015+j\,0.0046 & -0.0128+j0.0129 \\ -0.0108-j\,0.0269 & 0.015-j\,0.01 & 0.0067-j\,0.0023 & 0.0045-j\,0.0029 & 0.0172-j\,0.0043 & -0.0197+j\,0.0061 & -0.015-j\,0.0046 & 0.9334 & -0.0163+0.0019 \\ -0.0041-j\,0.0086 & 0.0212-j\,0.0006 & 0.0233+j\,0.0087 & 0.0262+j\,0.0007 & 0.0202-j\,0.0001 & -0.0187-j\,0.0034 & -0.0128-j\,0.0129 & -0.0163-j\,0.0019 & 0.9288 \end{bmatrix} \approx \begin{bmatrix} 1&0&0&0&0&0&0&0&0 \\ 0&1&0&0&0&0&0&0&0 \\ 0&0&1&0&0&0&0&0&0 \\ 0&0&0&1&0&0&0&0&0 \\ 0&0&0&0&1&0&0&0&0 \\ 0&0&0&0&0&1&0&0&0 \\ 0&0&0&0&0&0&1&0&0 \\ 0&0&0&0&0&0&0&1&0 \\ 0&0&0&0&0&0&0&0&1 \end{bmatrix} \quad (14)$$

3.2. The results of LHCP and RHCP of triangular array antennas 2×4

When the radiating patches and the modified lossless T-junction power divider 2×4 networks are run in the CST software, the results show in Figure 3 to Figure 9 for simulation of triangular array antenna 2×4, in the case of *S*-parameter, input impedance, frequency characteristic, radiation pattern, and antenna efficiency at around resonant frequency [14, 27]. Figure 3 shows the relationship between the reflection coefficient (S_{11} of the corporate feeding-line of array antenna) and the frequency for the simulation of LHCP and RHCP *Tx*/*Rx* triangular array antenna. From this figure, it can be seen that the S_{11} value and the S_{11} bandwidth at the resonant frequency, f = 1.25 GHz both LHCP and RHCP are about –23.13 dB and 36 MHz (2.88%), respectively.

Figure 4 depicts the input impedance characteristic of *Tx*/*Rx*. This figure shows that the real part of simulation at the resonant frequency of 1.25 GHz both of LHCP and RHCP is 50.15 **Ω**, close to the value of 50 **Ω**. The reactance part of this antenna is 7.02 **Ω**, and then it looks inductive. If we see the feed network, the length from each patch to input port should be fixed at l λ/4 (l = 1, 3, 5, etc.) to achieve the optimal current intensity [15]. In this work, we use l = 21. Figure 5 shows that the values of gain and axial ratio for simulation of triangular array antenna at the direction of θ = –36° (LHCP) and θ = 36° (RHCP) and the resonant frequency, f = 1.25 GHz are about 13.46 dBic and 1.99 dB, respectively. Moreover, the 12-dBic gain-bandwidth and the 3-dB *Ar*-bandwidth are consecutively around 38 MHz (3.04%) and 6 MHz (0.48%).

Figure 6 and Figure 7 depict the relationship between gain and elevation or θ-angle produced from the triangular array antenna (negative-θ for *Az* = 180° or 270° and positive-θ for *Az* = 0° or 90°) as azimuth direction of CP-SAR at f = 1.25 GHz (see Figure 6 for *Az* = 0° or *x*-*z* plane and Figure 7 for *Az* = 90° or *y*-*z* plane). At the elevation –36° (LHCP) and 36° (RHCP), the average of maximum gain and the axial ratio value of the triangular array antenna are about 13.49 dBic and 1.99 dB in both of azimuth angle, respectively. These figures also show that the beamwidth of the major lobes that exceed the target gain of 12 dBic both LHCP and RHCP are around 12°, from –42° to –30° (*Az* = 180° and *Az* = 270°or negative-θ) and from 30° to 42° (*Az* = 0° and *Az* = 90° or positive-θ). Moreover, the simulated 3-dB *Ar*-beamwidth both LHCP and RHCP are 38°, from –55° to –17° (*Az* = 180° and *Az* = 270°) and 53°, from 4° to 57° (*Az* = 0° and *Az* = 90°). The simulated gain-beamwidth of 12 dBic both LHCP and RHCP are achieved. The simulated 3-dB *Ar*-beamwidth for LHCP and RHCP are almost satisfied the targeted elevation beamwidth of 3.57°– 31.02° in Table 1 for better resolution of CP-SAR using UAV.

Figure 8 describes the characteristic of azimuth/conical pieces radiation generated by the triangular array antenna in the area of θ = –36° (LHCP) and θ = 36° (RHCP) at the resonant frequency of 1.25 GHz. From this figure, we can see that the peaks of the gain are 13.46 dBic at ϕ = 0° and 13.41 dBic at ϕ = 180°, while the axial ratio values of 1.89 dB at ϕ = 0° and 1.88 dB at ϕ = 180°. In addition, the values of the gain-beamwidth of 12 dBic are equal to 33° (from ϕ = 344° to ϕ = 17° and from ϕ = 164° to ϕ = 197°). While, the values of the axial ratio beamwidth of 3 dB are 95° (from ϕ = 310° to ϕ = 45°) and 87° (from ϕ = 137° to ϕ = 224°). These results exhibit that the targeted azimuth beamwidth of ≥ 6.77° obtains the resolution of CP-SAR using UAV. Figure 9 shows the antenna efficiency which means the radiation

efficiency for LHCP = 84.32% and RHCP = 84.33% on a target frequency of 1.25 GHz. These results indicate that the targeted antenna efficiency of 80% is achieved for CP-SAR using UAV.

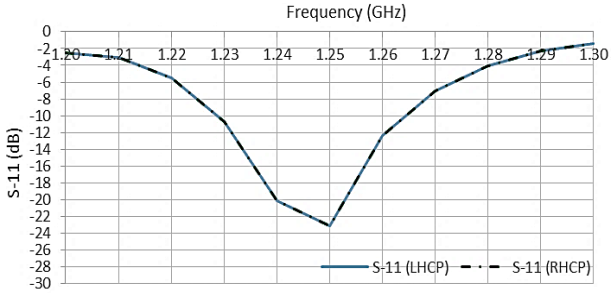

Figure 3. *S*-parameter, 2×4 patches

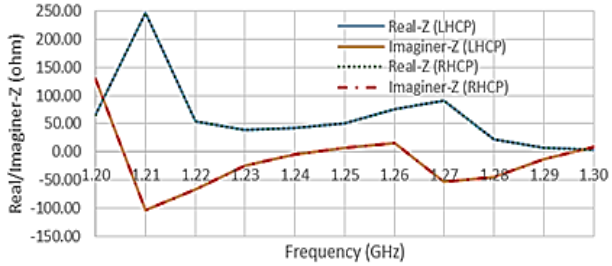

Figure 4. Input impedance, 2×4 patches

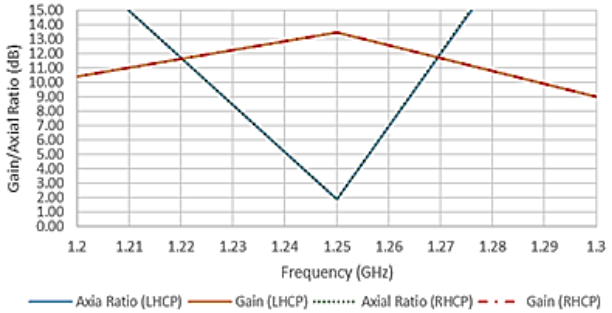

Figure 5. Frequency characteristic, 2×4 patches

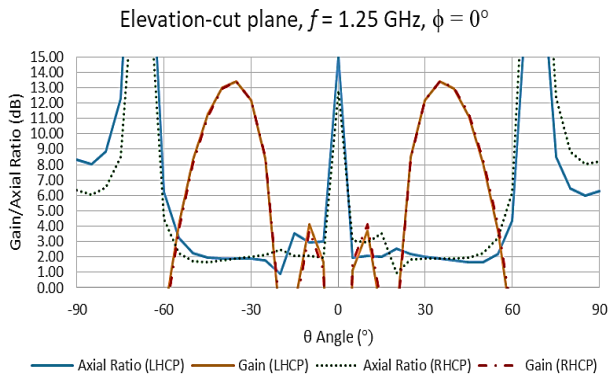

Figure 6. Elevation *x-z* plane, 2×4 patches

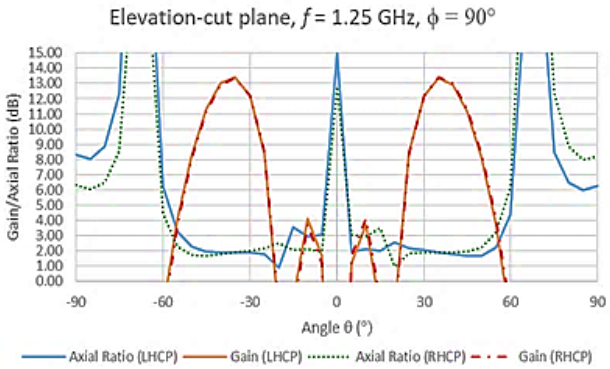

Figure 7. Elevation *y-z* plane, 2×4 patches

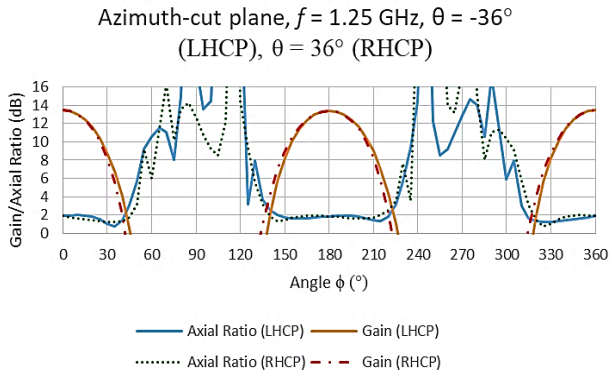

Figure 8. Conical *x-y* plane, 2×4 patches

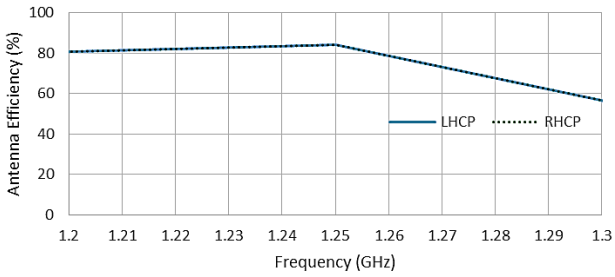

Figure 9. Antenna efficiency, 2×4 patches

4. CONCLUSION

The characteristics of LHCP and RHCP triangular array eight patches antennas using corporate feeding-line at *L*-band frequency have been studied for CP-SAR embedded on small UAV. In general, we obtained a good agreement between the simulated results and the technical specification of CP-SAR on UAV namely: (i) the values of gain and axial ratio (*Ar*) at the resonant frequency of both LHCP and RHCP were 13.46 dBic and 1.99 dB, respectively, (ii) the two-beams appearing on boresight in elevation plane had similar values for each other i.e. for average gain-beamwidth of 12 dBic and the 3-dB *Ar*-beamwidth were consecutively around 12° and 46° that exceed the targeted elevation beamwidth of 3.57°–31.02°. (iii) the average azimuth values of the gain-beamwidth of 12 dBic and *Ar*-beamwidth of 3 dB at the resonant frequency of 1.25 GHz and both θ = –36° (LHCP) and θ = 36° (RHCP) were 33° and 91°, respectively. These results exhibited that the targeted azimuth beamwidth of 6.77° achieved CP-SAR resolution with UAV. (iv) The antenna efficiency was about LHCP = 84.32% and RHCP = 84.33% on a target frequency of 1.25 GHz. These results indicated that the targeted antenna efficiency of 80% was achieved for CP-SAR using UAV.

REFERENCES

[1] Edwar and A. Munir, "Development of SAR transmitter for nanosatellite-based remote sensing application," *The 5th International Conference on Electrical Engineering and Informatics*, Bali, 2015.

[2] S. Salihah, et al., "A MIMO H-shape dielectric resonator antenna for 4G applications," *IJEECS*, vol. 10, no. 2, pp. 648-653, 2018.

[3] M. F. E. Purnomo and J. T. Sri Sumantyo, "Design circularly polarized of equilateral triangular hole antenna for SAR (synthetic aperture radar)," *IEICE Technical Report*, vol. 111, no. 239, 2011.

[4] J. T. Sri Sumantyo, "Development of circularly polarized synthetic aperture radar onboard unmanned aerial vehicle (CP-SAR UAV)," *IGARSS*, vol. 65, pp. 4762-4765, 2012.

[5] J. T. Sri Sumantyo and K. V. Chet, "Development of circularly polarized synthetic aperture radar onboard UAV for earth diagnosis," *EUSAR*, pp. 136-138, 2012.

[6] R. P. Silalahi, *et al.*, "Assessing the crown closure of nypa on UAV images using mean-shift segmentation algorithm," *IJEECS*, vol. 9, no. 3, pp. 722-730, 2018.

[7] M. Baharuddin, *et al*., "Equilateral microstrip antenna for circularly-polarized synthetic aperture radar," *Progress In Electromagnetics Research C*, vol. 8, pp. 107-120, 2009.

[8] Y. K. Chan and V. C. Koo, "The design and development of unmanned aerial vehicle synthetic aperture radar," *Progress In Electromagnetics Research Online*, vol. 7, no. 7, pp. 685-688, 2011.

[9] V. C. Koo, et al., "A new unmanned aerial vehicle synthetic aperture radar for environmental monitoring," *Progress in Electromagnetics Research*, vol. 122, pp. 245-268, 2012.

[10] A. Albert, *et al*., "ARBRES: Light-weight CW/FM SAR sensors for small UAVs," *Sensors*, vol. 13, no. 3, pp. 3204-3216, 2013.

[11] M. F. E. Purnomo, *et al*., "Development *L*-band antena with low power for circularly polarized-synthetic aperture radar (CP-SAR) application on unmanned aerial vehicle (UAV)," *Proceedings of the 7th Indonesia Japan Joint Scientific Symposium, the 24th CEReS International Symposium, the 4th Symposium on Microsatellite for Remote Sensing* (*SOMIRES 2016*), *the 1st Symposium on Innovative Microwave Remote Sensing, Keyaki Convention Hall*, pp. 392-403, 2016.

[12] C. L. Tang, et al., "Circularly polarized equilateral-triangular microstrip antenna with truncated-tip," *Electronics Letter*, vol. 34, no. 13, pp. 1227-1228, 1998.

[13] J. T. Sri Sumantyo, *et al*., "Development of circularly polarized synthetic aperture radar on-board microsatellite," *PIERS Proceedings*, pp. 382-385, 2009.

[14] M. F. E. Purnomo and A. Kitagawa, "Development of equilateral triangular array antenna with truncated-tip for circularly polarized-synthetic aperture radar sensor application," *Proceedings of 12th European Conference on Synthetic Aperture Radar*, 2018.

[15] A. Yohandri, et al., "Development of circularly polarized array antenna for synthetic aperture radar sensor installed on UAV," *Progress in Electromagnetics Research C*. vol. 19, pp. 119-133, 2011.

[16] C. E. Santosa, *et al*., "Subarray design for *C*-band circularly-polarized synthetic aperture radar antenna onboard airborne," *Progress in Electromagnetics Research*, vol. 163, pp. 107-117, 2018.

[17] M. F. E. Purnomo, et al., "Analysis performance of singly-fed circularly polarized microstrip antenna for wireless communication," *Jurnal Teknologi*, vol. 78, no. 5-9, pp. 111-117, 2016.

[18] CST Studio Suite 2016, "Microwave – Radio Frequency – Optical. Copyright © 1998 – 2016," *CST AG*, 2016.

[19] M. F. E. Purnomo, *et al*., "The array microstrip antenna for mobile-internet of satellite energy communication," *International Journal of Computer and Communication Engineering*, vol. 8, no. 3, pp. 119-128, 2019.

[20] J. M. Parenreng and A. Kitagawa, "Resource optimization techniques and security levels for wireless sensor networks based on the ARSy framework," *Sensors*, vol. 18, no. 1594, pp. 1-15, 2018.

[21] P. D. Prasetyo Adi and A. Kitagawa, "ZigBee radio frequency (RF) performance on raspberry Pi 3 for internet of things (IoT) based blood pressure sensors monitoring," (*IJACSA*) *International Journal of Advanced Computer Science and Applications*, vol. 10, no. 5, pp. 18-27, 2019.

[22] M. F. E. Purnomo and A. Kitagawa, "Triangular microstrip antenna for circularly-polarized synthetic aperture radar sensor application," *Indonesian Journal of Electrical Engineering and Computer Science*, vol. 12, no. 1, pp. 310-318, 2018.

[23] D. Pozar, "Microwave engineering," *John Wiley & Sons Inc. 3rd edition, Hoboken, New Jersey*, pp. 308-361, 2005.

[24] A. Grebennikov, "RF and microwave transmitter design," *John Wiley & Sons Inc., Hoboken, New Jersey*, 2011.

[25] K. Chang, "Encyclopedia of RF and microwave engineering," *John Wiley & Sons Inc., Hoboken, New Jersey*, 2005.

[26] M. F. E. Purnomo and A. Kitagawa, "Developing basic configuration of triangle array antenna for circularly polarized-synthetic aperture radar sensor application," *Proceedings of IEEE 2017 International Conference on Radar, Antenna, Microwave, Electronics, and Telecommunications* (*ICRAMET 2017*), pp. 112-117, 2017.

[27] I. Sukma and A. Kitagawa, "Comparison topologies of resonant tank from class-*C* wireless power transfer," *IEEE International Workshop on Electromagnetics*: *Applications and Student Innovation Competition* (*iWEM*), *Nagoya*, pp. 1-2, 2018.